Chemistry–A European Journal
Full Paper
doi.org/10.1002/chem.202004104
Chemistry Europe
European Chemical Societies Publishing

Materials Science | *Very Important Paper*

VIP A Simple Route to the Synthesis of Pt Nanobars and the Mechanistic Understanding of Symmetry Reduction

Ruhui Chen,[a] Quynh N. Nguyen,[b] Ming Zhao,[a] Zitao Chen,[c, d] Miaofang Chi,[d] and Younan Xia*[a, c]

Abstract: Noble-metal nanocrystals with anisotropic shapes have received increasing interest owing to their unique properties. Here, a facile route to the preparation of Pt nanobars with aspect ratios tunable up to 2.1 was reported by simply reducing a Pt^{IV} precursor in *N*,*N*-dimethylformamide (DMF) at 160 °C in the presence of poly(vinyl pyrrolidone) (PVP). In addition to its commonly observed roles as a solvent and a reductant, DMF could also decompose to generate CO, a capping agent capable of selectively passivating Pt{100} facets to promote the formation of nanobars. The size and aspect ratio of the nanobars could be tuned by varying the amount of Pt^{IV} precursor involved in the synthesis, as well as the concentration of PVP because of its dual roles as a stabilizer and a co-reductant. Our mechanistic study indicated that the anisotropic growth resulted from both particle coalescence and localized oxidative etching followed by preferential growth.

Introduction

The successful synthesis of noble-metal nanocrystals with diverse shapes offers exciting opportunities in a wide variety of applications.[1] Even if enclosed by the same crystallographic facets, nanocrystals taking different geometric shapes could still exhibit different properties and performances.[1a,2] A notable example can be found in the surface-enhanced Raman scattering (SERS) property of Ag nanobars, which is highly dependent on their aspect ratio.[3] A nanobar is enclosed by six {100} side faces similar to a nanocube, but elongated along one (or two) direction with an aspect ratio greater than one. Besides the unique features in plasmonics, nanobars might also exhibit attractive catalytic properties. Although the type of facet or surface structure of nanocubes and nanobars is essentially identical, their difference in specific surface area and the proportion of undercoordinated atoms situated on edges and corners can lead to distinct catalytic performance.[1a] For example, the Pt nanobar exhibited different CO poisoning tolerance in methanol oxidation reaction as its aspect ratio varied, but the mechanism is yet to be resolved.[4] Moreover, by enlarging the area in contact with the support, it is expected that the movement and detachment of nanobars will be mitigated under the harsh electrochemical conditions, enabling higher durability, as reported for catalysts based on one-dimensional metal nanocrystals.[5]

Despite the attractive properties of nanobars, it is challenging to induce anisotropic growth during a colloidal synthesis of noble-metal nanocrystals, owing to the constraint from their face-centered cubic (*fcc*) lattice.[6] Enclosed by multiple equivalent facets possessing surface atoms with the same spatial arrangement and coordination number, there is no intrinsic driving force for an *fcc* metal to break its cubic symmetry and grow into an anisotropic shape. To this end, a variety of strategies have been proposed and demonstrated for generating nanobars, including particle attachment,[4,7] facet-selected growth as a result of localized oxidative etching,[3,8] and manipulation of reduction kinetics.[9] Although progress has been made in the synthesis of nanobars, the available synthetic methods and understanding of the mechanism responsible for anisotropic growth and symmetry reduction are still limited, compared with other types of one-dimensional nanostructures, let alone nanocrystals taking isotropic shapes. To promote the potential applications of nanobars, it is of critical importance to deepen our understanding in symmetry reduction for achieving anisotropic growth in a controllable manner.

Most of the synthetic protocols that have been developed so far focus on the preparation of Pd,[7,8,10] Ag,[3,9,11] and bimetallic[12] nanobars. As for Pt, although it has been demonstrated as a key catalytic material for a number of reactions and indus-

[a] *R. Chen, M. Zhao, Prof. Dr. Y. Xia*
School of Chemistry and Biochemistry, Georgia Institute of Technology
Atlanta, Georgia 30332 (USA)
E-mail: younan.xia@bme.gatech.edu
[b] *Q. N. Nguyen*
Department of Chemistry, Agnes Scott College
Decatur, Georgia 30030 (USA)
[c] *Z. Chen, Prof. Dr. Y. Xia*
The Wallace H. Coulter Department of Biomedical Engineering
Georgia Institute of Technology and Emory University
Atlanta, Georgia 30332 (USA)
[d] *Z. Chen, Dr. M. Chi*
Center for Nanophase Materials Sciences, Oak Ridge National Laboratory
Oak Ridge, Tennessee 37831 (USA)
Supporting information and the ORCID identification number(s) for the author(s) of this article can be found under: https://doi.org/10.1002/chem.202004104.

trial processes,[1a] limited success has been achieved in the synthesis of Pt nanobars with well-defined facets and controlled aspect ratio.[4,8] Due to the difference in intrinsic properties among various metals, the synthetic method for Pt nanobars tends to differ from those developed for other metals and thus need further study. In an early report, it was demonstrated that Pt nanobars could be prepared by reducing Na_2PtCl_6 in a mixture of ethylene glycol and water in the presence of KBr and poly(vinyl pyrrolidone) (PVP).[8] The localized oxidative etching enabled by the Cl^-/O_2 pair selectively removed Br^- ions from one of the side faces on a cube to activate the preferential growth for the generation of nanobars. However, the product quality was poor. In another study, Pt nanobars were obtained through the reduction of $Pt(acac)_2$ by benzyl alcohol at 180 °C in the presence of oleylamine and formaldehyde as the capping agents.[4] It was proposed that particle coalescence contributed to the formation of Pt nanobars, and the aspect ratio could be tuned by varying the amount of formaldehyde. However, the explicit roles played by the reactants in the anisotropic growth and the mechanism for the control over aspect ratio are still ambiguous.

Herein, we report a facile synthesis of Pt nanobars by heating a Pt^{IV} precursor in *N*,*N*-dimethylformamide (DMF) in the presence of PVP. In addition to its common roles as a solvent and a reductant, DMF plays a critical role in the formation of Pt nanobars by producing a capping agent in situ. Specifically, CO from the decomposition of DMF at an elevated temperature can act as a capping agent selective toward Pt{100} facets, facilitating the formation of Pt nanobars. The aspect ratio and size of the nanobars can be tuned by simply adjusting the concentrations of the precursor and PVP involved in the synthesis. Besides the explicit roles played by the reactants in the synthesis, we also uncover the mechanisms responsible for the formation of nanobars. Our mechanistic study indicates that both particle coalescence and localized oxidative etching followed by preferential growth contribute to the anisotropic growth vital in the formation of nanobars.

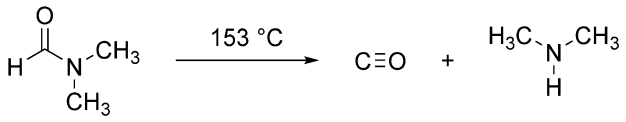

Scheme 1. Decomposition of DMF at its boiling point (or a higher temperature) to produce CO.

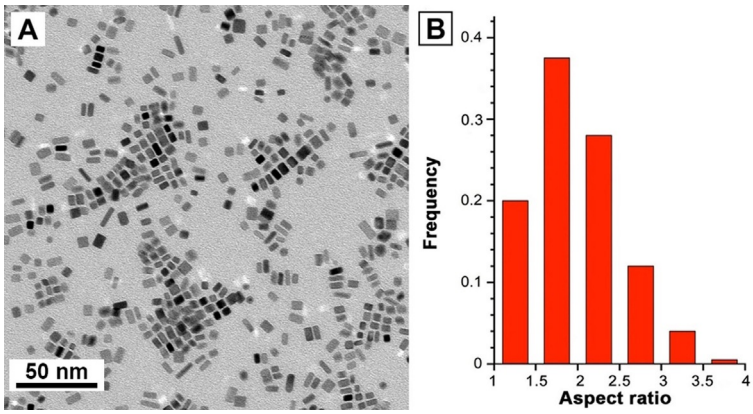

Figure 1. (A) Typical TEM image and (B) distribution of the aspect ratio (length/width) of the Pt nanobars prepared using the standard protocol.

Results and Discussion

In a standard synthesis, the Pt^{IV} precursor was reduced by DMF in an oil bath held at 160 °C in the presence of PVP, which could serve the dual roles as a stabilizer and a mild reducing agent. Although the temperature of the oil bath was higher than the normal boiling point of DMF (153 °C), the reaction solution did not boil during the synthesis, probably due to the increased pressure inside the tightly capped vial. It was expected that DMF would decompose at such a high temperature to produce CO (see Scheme 1), a capping agent selective toward the Pt{100} facets. Figure 1 A shows a representative transmission electron microscopy (TEM) image of the Pt nanobars obtained using the standard procedure. Specifically, about 90% of the particles in this product showed a bar-like morphology. The average length, width, and aspect ratio of the Pt nanobars were 8.0 ± 1.5, 4.2 ± 0.9, and 2.0 ± 0.5 nm, respectively (Figure 1 B). It should be pointed out that the size measurements were based upon TEM images, and some Pt nanocrystals with a square projection could also be nanobars vertically oriented on the copper grid. As such, the purity of the sample tends to be underestimated, and the actual distribution of aspect ratios should be narrower.

By changing the concentration of the precursor in the solution, the size and aspect ratio of the Pt nanobars could be readily tuned by varying the number of seeds formed during nucleation and the amount of precursor available for the growth step. Figure S1 shows TEM images of the Pt nanobars prepared when the amount of the Pt^{IV} precursor was varied in the range of 2–40 mg. When the amount of the Pt^{IV} precursor was increased from 20 mg in the standard procedure to 40 mg, the product had a slightly lower aspect ratio of 1.8 and a smaller edge length of 5.1 nm (Figure S1A). In this case, more seeds were formed during nucleation because of the substantially accelerated initial reduction rate. As the amount of precursor introduced into the synthesis was fixed, a smaller amount of the precursor would be allocated to each seed for the following growth process, giving rise to nanobars with a smaller size and a lower aspect ratio. When the amount of the precursor was further decreased to 10 mg, the edge length of the Pt nanobars slightly decreased to 7.3 nm while the aspect ratio was reduced to 1.4 (Figure S1B). A plausible explanation is that when the concentration of the precursor was low, fewer seeds would be generated in the nucleation step, but the small amount of precursor remained in the solution might not be adequate for the anisotropic growth of the already formed seeds. As a result, the nanobars would take a smaller size and aspect ratio. Therefore, nanobars with the greatest aspect ratio were only obtained when the amount of the precursor was op-

timized to 20 mg as used in the standard protocol. This explanation is consistent with the proposed growth mechanism, which will be discussed at a later point. Interestingly, as the amount of the precursor was further decreased to 5 and 2 mg, as shown in Figure S1C, D, nanocubes and nanocrystals with irregular shapes became the dominant species in the product. The change could be ascribed to a much slower reduction rate due to the extremely low concentration of the precursor, leading to the generation of diverse seeds during the nucleation stage and their growth into particles with irregular shapes.

Since its terminal hydroxy groups have the reducing capability, PVP can serve the dual roles as a stabilizer and a mild reducing agent in the synthesis of Pt nanocrystals.[13] To validate the role of PVP in the synthesis of Pt nanobars, the amount of PVP introduced into the reaction was varied while keeping all the other parameters fixed. Figure S2 shows TEM images of Pt nanobars prepared using the standard protocol except that different amounts of PVP were involved. As shown in Figure S2A, B, changes to the Pt nanobars were not obvious when the amount of PVP was decreased from 100 mg in the standard protocol to 50 mg, while a slight increase in size to 8.7 nm and aspect ratio to 2.1 was observed when 20 mg of PVP was used. The increase in size and aspect ratio could be attributed to a slower reduction rate at an extremely low concentration of PVP, leading to the formation of fewer seeds in the early stage of the synthesis. In the growth process, more precursor would be available for growth, resulting in the enlargement of Pt nanobars. As expected, when the amount of PVP was increased to 200 and 400 mg (Figure S2C, D), smaller Pt nanobars with average edge length of 6.2 and 4.2 nm, and aspect ratios of 1.6 and 1.4, respectively, were formed in addition to some small particles. This can be rationalized by the stronger reducing power at a higher concentration of PVP, leading to the formation of a larger number of seeds and thus a smaller size for the resultant nanobars. Moreover, self-nucleation occurred due to the accelerated reduction of the precursor, generating some small particles. Taken together, we can conclude that PVP did not just act as a stabilizer to prevent the nanocrystals from agglomeration; it could also serve as a mild reducing agent in the reaction. Collectively, by varying the concentrations of the Pt^{IV} precursor and PVP, Pt nanobars with tunable sizes in the range of 4.2 to 8.7 nm and aspect ratios ranging from 1.4 to 2.1 could be obtained.

In this synthesis, DMF acted as a solvent, a reducing agent, and a precursor to the actual capping agent. A number of protocols involving DMF have been reported for the synthesis of colloidal metal nanocrystals with different shapes, including Pd tetrahedra,[14] Ag decahedra and icosahedra,[15] and Au decahedra,[16] among others. In most of these studies, DMF was simply regarded as a solvent or a reducing agent. A few studies, however, demonstrated that DMF could play the role of a capping agent to affect the shape taken by the metal nanocrystals. For example, it was proposed that DMF or its oxidation product could serve as a capping agent responsible for the generation of Au rhombic dodecahedra covered by {110} facets.[17] Moreover, a recent study revealed that DMF was critical to the formation of ultrathin Pt nanowires because it could react with water to produce H_2 and thus induce the coalescence of Pt nanoparticles.[18] In the present work, in addition to its common roles as a solvent and a reductant, DMF played an essential role in the formation of Pt nanobars enclosed by {100} facets. At its normal boiling point of 153 °C or a higher temperature, DMF would decompose to produce CO and dimethylamine (Scheme 1).[19]

It has been well documented that CO could serve as a capping agent selective toward the Pt{100} facets.[20] A recent study on the synthesis of Pt nanocrystals by heating $Pt(acac)_2$ in oleic acid also demonstrated that CO arising from the decarbonylation of oleic acid contributed to the formation of Pt nanocubes and nanobars enclosed by {100} facets.[21] Besides the capping effect, CO could also act as a reducing agent in the synthesis, facilitating the nucleation and growth processes. To confirm the presence of CO on the surface, Fourier-transform infrared (FTIR) spectroscopy was performed on the as-synthesized Pt nanobars. As shown in Figure 2, the FTIR spectrum exhibited a well-resolved band at 1990 cm^{-1} and a weak band at 1824 cm^{-1}, corresponding to the linear and bridging CO species, respectively.[20b] The absence of these two bands on the FTIR spectra of PVP and DMF indicates that they were not from the residual PVP or DMF remaining in the sample. It can be concluded that the CO generated from the decomposition of DMF served as a capping agent for the Pt{100} facets, and likely a reducing agent as well, contributing to the formation of Pt nanobars. Different from previous reports on the synthesis of Pt nanocubes, during which metal carbonyls[22] or CO gas flow[20b] was introduced into the reaction system, DMF in this simple route not only served as a solvent and a reductant, but also generated CO in situ for the selective capping toward Pt{100}. As expected, when DMF was replaced by benzyl alcohol and ethylene glycol (Figure S3), Pt nanoparticles with nearly spherical shapes were obtained, suggesting the pivotal role of DMF as a source of capping agent in the formation of Pt nanobars.

Since there is no intrinsic driving force for the Pt nanocrystals to grow into an anisotropic shape lower in symmetry than its cubic lattice, we were interested in understanding the mechanism responsible for the formation of the Pt nanobars. To gain insight into the shape evolution and thus elucidate the mechanism underlying the anisotropic growth, the nanocrystals formed at different time points during the standard synthesis were collected and examined by TEM. Figure 3 shows TEM images of the intermediates that reveal the morphological evolution of the nanocrystals from small seeds to nanobars. As shown in Figure 3A, a large number of small seeds were formed at the initial stage of the synthesis ($t = 2$ h). At $t = 2.5$ h (Figure 3B), in addition to more particles with sizes smaller than 3 nm, some relatively large bar-shaped particles and truncated cubes were observed. As the reaction proceeded to $t =$ 3.5 h (Figure 3C), anisotropic growth could be clearly identified as almost all of the nanocubes and the large particles evolved into bar-shaped structures with an average aspect ratio of 1.2, while the number of small particles decreased significantly. If the reaction was allowed to continue for 6 h (Figure 3D), all the small particles disappeared from the product, and the re-

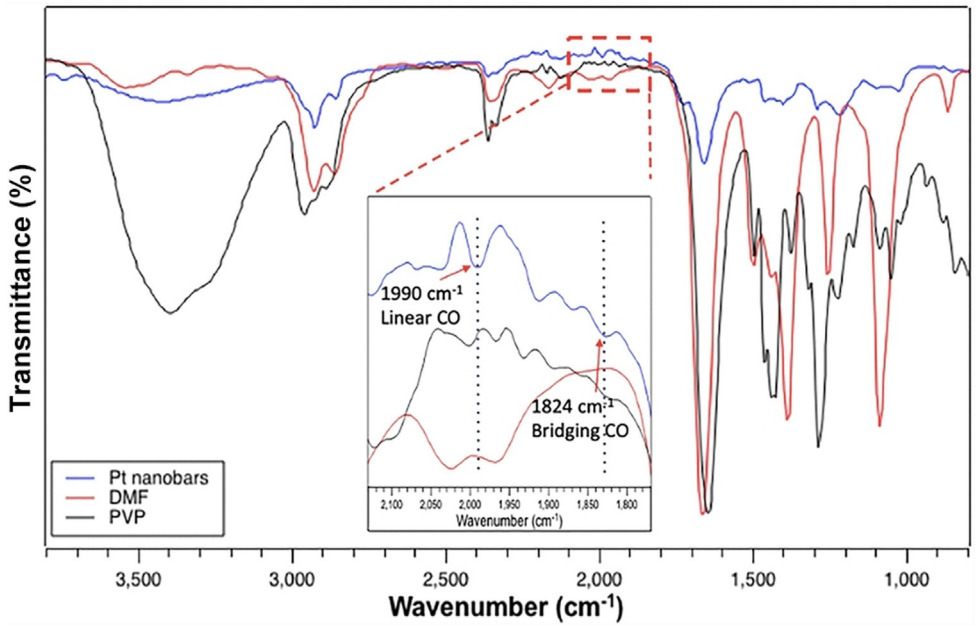

Figure 2. FTIR spectra of the Pt nanobars prepared using the standard protocol, confirming the presence of CO on the surface of the nanobars by showing well-resolved CO bands corresponding to the linear and bridging configurations.

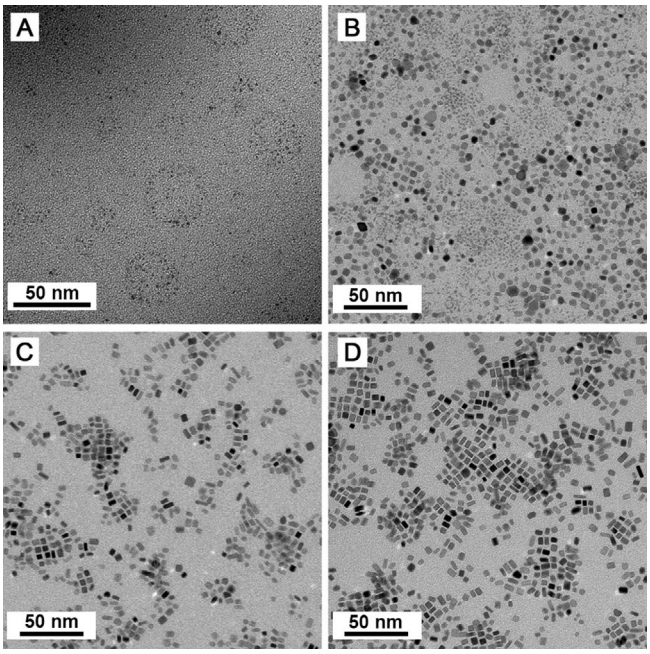

Figure 3. TEM images of Pt nanocrystals obtained at different time points of a standard synthesis: (A) 2, (B) 2.5, (C) 3.5, and (D) 6 h, respectively.

maining Pt nanobars exhibited sharp edges and corners, as well as an increase in aspect ratio to 1.6.

The presence of both bar-shaped and cubic nanocrystals in the sample obtained at $t = 2.5$ h led us to postulate that two different growth pathways could be involved in the formation of Pt nanobars. A careful examination of the sample by high-resolution TEM (HRTEM) revealed that the existence of the bar-shaped nanocrystals at the early stage of the synthesis could be ascribed to the coalescence of the initially formed small Pt nanoparticles. Figure 4A shows HRTEM image of two Pt nanocrystals featuring a bar-like shape and continuous lattice fringes, validating their single-crystal structure. In addition, the attachment of two adjacent small Pt nanoparticles was also clearly observed in this sample (Figure 4B-D), demonstrating the occurrence of particle coalescence. It is noteworthy that nanoparticles formed at the beginning of the reaction would be single-crystal while particles with twin defects could be generated as the reduction rate slowed down due to the continuous consumption of the Pt precursor. However, in the presence of Cl^- ions released from the precursor and O_2 dissolved in the solution, the twinned particles would be selectively removed afterwards as a result of oxidative etching,[6a] leaving behind single-crystal nanoparticles. From the thermodynamic point of view, the small Pt nanoparticles with great mobility and high surface energy would like to collide and attach to each other to reduce the total surface free energy. The two nanoparticles could rotate to join with the lattice planes sharing the same crystallographic orientation (Figure 4B), leading to the formation of larger nanocrystals with a single-crystal structure. On the other hand, when the particles attach in an orientation-mismatched manner, as indicated by the domain boundaries in between (Figure 4C, D), defects would be included in the resultant particle. Despite the polycrystallinity of the coalesced particle, recrystallization could take place afterwards, during which the defects would be eliminated, and the surface of the nanocrystals would be smoothed via lattice rotation and atom migration in the presence of capping agent. The reconstruction in structure and shape by recrystallization has also been observed in the formation of Pd, Pt, and PtFe nanocrystals.[7,23] Moreover, the involvement of recrystallization in the growth of nanobars is also suggested by the fact that slight kinks were observed in Pt nanobars formed in the early stage

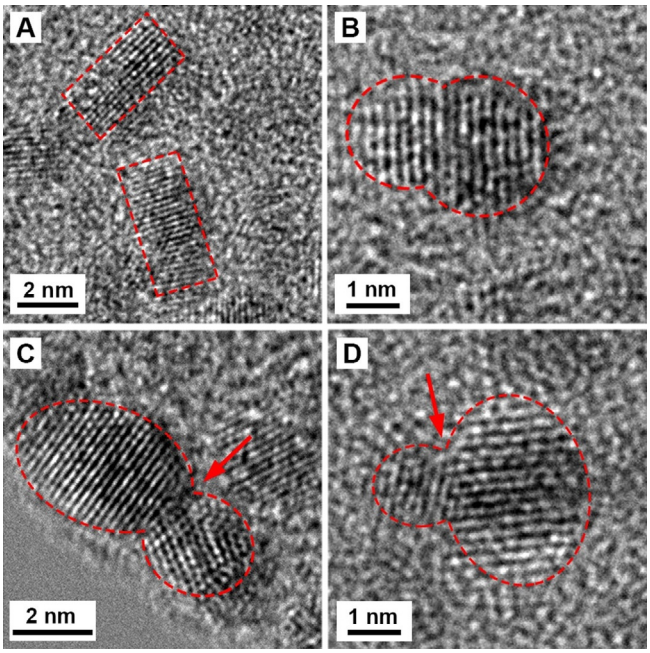

Figure 4. HRTEM images of the product obtained at $t = 2.5$ h into a standard synthesis showing (A) small Pt nanocrystals with a bar-like shape and single-crystal structure and (B–D) Pt nanoparticles coalesced in (B) an orientation matched and (C, D) mismatched manner. The red dashed line outlines the profile of the particles while the arrow indicates the domain boundary between the Pt nanoparticles.

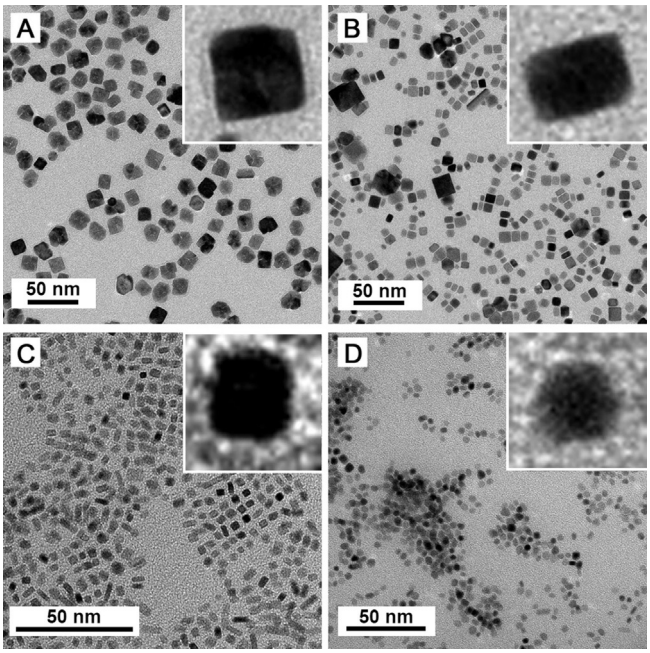

Figure 5. TEM images of Pt nanocrystals prepared using the standard procedure except for the different precursors and atmospheres: (A) $Pt(acac)_2$, (B) $Pt(NH_3)_2Cl_2$, (C) $Na_2PtCl_6{\cdot}6H_2O$ together with bubbling Ar into the reaction solution, and (D) $Na_2PtCl_6{\cdot}6H_2O$ with the addition of 0.13 M citric acid, respectively. Insets are magnified TEM images of individual Pt nanocrystals.

of a synthesis (e.g., the particle at the bottom of Figure 4A) while nanobars with well-defined shape were obtained as the final product. Taken together, particle coalescence followed by recrystallization of the attached particle in the presence of CO as a capping agent led to symmetry breaking and elongation of Pt nanocrystals along one dimension, giving rise to single-crystal nanobars enclosed by {100} facets. A similar mechanism involving the particle coalescence was also suggested for the formation of Pd nanobars synthesized in an aqueous solution by a different procedure.[7]

In addition to particle coalescence, the formation of nanobars could also be attributed to the anisotropic growth of nanocubes driven by localized oxidative etching. It was reported that localized oxidative etching was capable of breaking the symmetry of a nanocrystal through site-selective activation of the nanocrystal surface.[8] In this route, oxidative etching occurs locally on a specific face of the nanocrystal in the presence of an oxidant/ligand pair, such as O_2 and halide ions released from the precursor or other additives.[6a] By selectively removing the capping agent from the surface of nanocrystals, the activated site would be preferred for the deposition of atoms in the following growth, resulting in symmetry breaking. To validate the role of localized oxidative etching in the growth of Pt nanobars, we conducted the synthesis by following the standard protocol except that different types of precursors were used and the atmosphere in the reaction was also changed. As shown in Figure 5A, by replacing Na_2PtCl_6 with $Pt(acac)_2$ that contained no Cl^- ions, the as-obtained nanocrystals exhibited a nearly cubic shape. In contrast, the nanocrystals prepared with $Pt(NH_3)_2Cl_2$ as the precursor (Figure 5B) showed poor purity and uniformity but still contained a portion of nanobars, demonstrating the significance of Cl^- ions in the generation of nanobars. Furthermore, we conducted the synthesis under an inert atmosphere by bubbling the reaction solution with Ar to elucidate the role of oxygen. Although it is difficult to completely exclude oxygen from the reaction solution, the as-obtained products contained Pt nanocubes and nanobars with lower aspect ratios (Figure 5C), suggesting partial inhibition of anisotropic growth because of the reduced amount of O_2 in the reaction. Moreover, previous studies have reported that citric acid could efficiently block oxidative etching in the synthesis of nanocrystals due to its capability to react with and thus remove the adsorbed O_2.[8,24] Following this strategy, we added citric acid at a concentration of 0.13 M to the standard synthesis. The resultant product was found to consist of nanocubes and rounded nanoparticles (Figure 5D), indicating impeded anisotropic growth due to the lack of oxidative etching. A possible explanation for the presence of rounded nanoparticles is the strong binding of citric acid to Pt{111} facets, which may hinder the adsorption of CO on Pt surface and thus the generation of {100} facets. Taken together, the presence of O_2 and Cl^- ions released from the precursor is essential to the formation of Pt nanobars, attesting the significant role of localized oxidative etching in the induction of anisotropic growth.

Based on the experimental results, the growth mechanism for Pt nanobars was proposed as illustrated in Figure 6. At the beginning of the synthesis, the Pt^{IV} precursor was reduced by DMF at 160 °C with PVP serving as a co-reductant, generating

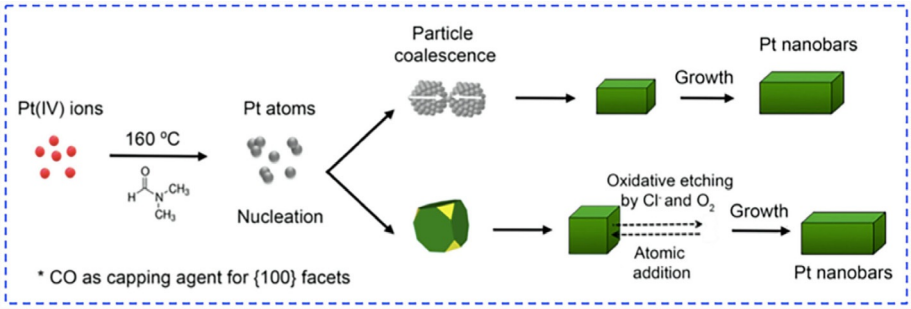

Figure 6. Schematic illustration of the proposed growth pathways of Pt nanobars. With CO serving as the capping agent for Pt{100} facets, the particle coalescence and localized oxidative etching followed by preferential growth both contributed to the anisotropic growth of Pt nanobars.

nuclei that then quickly evolved into small nanoparticles. Owing to the decomposition of DMF, CO was produced and acted as a capping agent for Pt{100} facets. Afterwards, two distinctive pathways could be taken for the generation of Pt nanobars. Due to the coalescence of the initially formed small nanoparticles, nanocrystals with larger sizes and bar-shaped morphology were formed, which later grew into nanobars with well-defined facets through recrystallization with the capping effect from CO.

Meanwhile, nanocubes were generated from the growth of the initially formed seeds, and localized oxidative etching started to take place. The Cl^- ions released from the precursor and O_2 in the solution could remove CO on the surface of a nanocube by oxidation. Without the capping agent as a physical barrier to prevent the addition of atoms onto the surface, this particular site was activated, favoring the deposition of Pt atoms. Once heterogeneous nucleation selectively occurred on one of the side faces, the following growth would preferentially take place on the activated surface, breaking the symmetry of a nanocube. As a result, anisotropic growth was triggered, promoting the elongation along one direction to generate nanobars. Taken together, the formation of Pt nanobars could be ascribed to the coalescence of small particles in the early stage of the synthesis and the preferential growth on specific faces of nanocubes activated by localized oxidative etching.

Conclusions

We have demonstrated a facile approach to the preparation of Pt nanobars by heating a Pt^{IV} precursor in *N*,*N*-dimethylformamide (DMF) with poly(vinyl pyrrolidone) (PVP) serving as a stabilizer and a mild reducing agent. The involvement of DMF is critical to the generation of nanobars as DMF played multiple roles in the synthesis: a solvent, a reducing agent, and a precursor for generating the capping agent in situ. Using Fourier-transform infrared (FTIR) spectroscopy, it was confirmed that CO, which was produced from the decomposition of DMF at a high temperature of 160 °C, served as the capping agent to selectively adsorb on {100} facets for the formation of Pt nanobars. By varying the concentrations of the Pt^{IV} precursor and PVP involved in the synthesis, the aspect ratio and size of the Pt nanobars could be readily tuned. It was found that the anisotropic growth was induced by both particle coalescence during the early stage of the synthesis and localized oxidative etching followed by further preferential growth. This work offers not only a facile route to the synthesis of Pt nanobars with well-defined facets and tunable aspect ratios, but also a deeper understanding of the growth mechanism responsible for metal nanocrystals to take shapes lower in symmetry relative to the cubic lattice.

Experimental Section

Chemicals and materials

Sodium hexachloroplatinate(IV) hexahydrate ($Na_2PtCl_6{\cdot}6H_2O$, 98%) and PVP ($M_w \approx 55000$) were obtained from Sigma–Aldrich. DMF (99.8%) was purchased from Acros Organics. All chemicals were used as received without further purification. Deionized water with a resistivity of 18.2 MΩ·cm was used throughout the experiments.

Synthesis of Pt nanobars

In a standard procedure, 20 mg of $Na_2PtCl_6{\cdot}6H_2O$ and 100 mg of PVP were dissolved in 10 mL of DMF under ultrasonication. The as-obtained yellow solution was stored in a tightly capped 20-mL glass vial and heated in an oil bath held at 160 °C for 16 h under magnetic stirring. The solid product was collected by centrifugation at 6000 rpm for 10 min and then washed with water twice to remove excess PVP. The Pt nanobars were then re-dispersed in water for further characterization.

Characterization

TEM images were taken using a Hitachi HT-7700 microscope operated at 120 kV. HRTEM images were captured on a Cs-corrected FEI Titan 80 kV TEM at the Oak Ridge National Laboratory (ORNL). FTIR spectra were performed on a Varian 640 spectrometer through the use of an attenuated total reflectance (ATR) accessory. The Pt nanobars for FTIR analysis were collected by centrifugation and re-dispersed in ethanol without further treatment. The sample was drop-cast on top of the crystal and dried under ambient conditions. The spectra were recorded in the range of 4000–400 cm^{-1} with a resolution of 8 cm^{-1}.

Acknowledgements

This work was supported in part by a research grant from the NSF (CHE-1804970) and start-up funds from the Georgia Insti-

tute of Technology. Q.N. acknowledges summer support from the NSF Research Experiences for Undergraduates (REU, CHE-1560335). TEM imaging was performed at the Georgia Tech Institute for Electronics and Nanotechnology, a member of the National Nanotechnology Coordinated Infrastructure (NNCI), which is supported by the National Science Foundation (ECCS-2025462). HRTEM images were acquired at the Oak Ridge National Laboratory's Center for Nanophase Materials Sciences sponsored by the U. S. Department of Energy Office of Science User Facility.

Conflict of interest

The authors declare no conflict of interest.

Keywords: CO-mediated synthesis · localized oxidative etching · particle coalescence · Pt nanobars · symmetry breaking

[1] a) Y. Shi, Z. Lyu, M. Zhao, R. Chen, Q. N. Nguyen, Y. Xia, *Chem. Rev.* **2020**, https://doi.org/10.1021/acs.chemrev.0c00454; b) A. Zada, P. Muhammad, W. Ahmad, Z. Hussain, S. Ali, M. Khan, Q. Khan, M. Maqbool, *Adv. Funct. Mater.* **2020**, *30*, 1906744; c) E. C. Dreaden, A. M. Alkilany, X. Huang, C. J. Murphy, M. A. El-Sayed, *Chem. Soc. Rev.* **2012**, *41*, 2740 – 2779; d) J. Zhang, Q. Kuang, Y. Jiang, Z. Xie, *Nano Today* **2016**, *11*, 661 – 677.

[2] S.-I. Choi, J. A. Herron, J. Scaranto, H. Huang, Y. Wang, X. Xia, T. Lv, J. Park, H.-C. Peng, M. Mavrikakis, Y. Xia, *ChemCatChem* **2015**, *7*, 2077 – 2084.

[3] Q. Zhang, C. H. Moran, X. Xia, M. Rycenga, N. Li, Y. Xia, *Langmuir* **2012**, *28*, 9047 – 9054.

[4] Y. Li, T. Bian, J. Du, Y. Xiong, F. Zhan, H. Zhang, D. Yang, *CrystEngComm* **2014**, *16*, 8340 – 8343.

[5] a) Y. Lu, Y. Jiang, W. Chen, *Nano Energy* **2013**, *2*, 836 – 844; b) M. Li, Z. Zhao, T. Cheng, A. Fortunelli, C.-Y. Chen, R. Yu, Q. Zhang, L. Gu, B. V. Merinov, Z. Lin, E. Zhu, T. Yu, Q. Jia, J. Guo, L. Zhang, W. A. Goddard III, Y. Huang, X. Duan, *Science* **2016**, *354*, 1414 – 1419; c) H. Huang, A. Ruditskiy, S.-I. Choi, L. Zhang, J. Liu, Z. Ye, Y. Xia, *ACS Appl. Mater. Interfaces* **2017**, *9*, 31203 – 31212.

[6] a) Y. Xia, Y. Xiong, B. Lim, S. E. Skrabalak, *Angew. Chem. Int. Ed.* **2009**, *48*, 60 – 103; *Angew. Chem.* **2009**, *121*, 62 – 108; b) A. R. Tao, S. Habas, P. Yang, *Small* **2008**, *4*, 310 – 325.

[7] B. Lim, H. Kobayashi, P. H. C. Camargo, L. F. Allard, J. Liu, Y. Xia, *Nano Res.* **2010**, *3*, 180 – 188.

[8] Y. Xiong, H. Cai, B. J. Wiley, J. Wang, M. J. Kim, Y. Xia, *J. Am. Chem. Soc.* **2007**, *129*, 3665 – 3675.

[9] S. Zhou, D. S. Mesina, M. A. Organt, T.-H. Yang, X. Yang, D. Huo, M. Zhao, Y. Xia, *J. Mater. Chem. C* **2018**, *6*, 1384 – 1392.

[10] a) Y. Yu, Y. Zhao, T. Huang, H. Liu, *Mater. Res. Bull.* **2010**, *45*, 159 – 164; b) B. Lim, M. Jiang, J. Tao, P. H. C. Camargo, Y. Zhu, Y. Xia, *Adv. Funct. Mater.* **2009**, *19*, 189 – 200.

[11] a) B. J. Wiley, Y. Chen, J. M. McLellan, Y. Xiong, Z.-Y. Li, D. Ginger, Y. Xia, *Nano Lett.* **2007**, *7*, 1032 – 1036; b) B. Wiley, Y. Sun, Y. Xia, *Acc. Chem. Res.* **2007**, *40*, 1067 – 1076.

[12] a) R. Carrera-Cerritos, C. Ponce de León, J. Ledesma-García, R. Fuentes-Ramírez, L. G. Arriaga, *RSC Adv.* **2014**, *4*, 16632 – 16640; b) K. Zhang, Y. Xiang, X. Wu, L. Feng, W. He, J. Liu, W. Zhou, S. Xie, *Langmuir* **2009**, *25*, 1162 – 1168.

[13] Y. Xiong, I. Washio, J. Chen, H. Cai, Z.-Y. Li, Y. Xia, *Langmuir* **2006**, *22*, 8563 – 8570.

[14] Y. Zhang, M. Wang, E. Zhu, Y. Zheng, Y. Huang, X. Huang, *Nano Lett.* **2015**, *15*, 7519 – 7525.

[15] a) M. Tsuji, M. Ogino, R. Matsuo, H. Kumagae, S. Hikino, T. Kim, S.-H. Yoon, *Cryst. Growth Des.* **2010**, *10*, 296 – 301; b) Y. Gao, P. Jiang, L. Song, J. X. Wang, L. F. Liu, D. F. Liu, Y. J. Xiang, Z. X. Zhang, X. W. Zhao, X. Y. Dou, S. D. Luo, W. Y. Zhou, S. S. Xie, *J. Cryst. Growth* **2006**, *289*, 376 – 380.

[16] A. Sánchez-Iglesias, I. Pastoriza-Santos, J. Pérez-Juste, B. Rodríguez-González, F. J. García de Abajo, L. M. Liz-Marzán, *Adv. Mater.* **2006**, *18*, 2529 – 2534.

[17] G. H. Jeong, M. Kim, Y. W. Lee, W. Choi, W. T. Oh, Q. H. Park, S. W. Han, *J. Am. Chem. Soc.* **2009**, *131*, 1672 – 1673.

[18] Y. Liu, C. Wang, W. Wang, R. Guo, W. Bi, Y. Guo, M. Jin, *Nanoscale* **2019**, *11*, 14828 – 14835.

[19] S. Creager, *Solvents and Supporting Electrolytes in Handbook of Electrochemistry* (Ed: C. G. Zoski), Elsevier, Amsterdam, **2007**, pp. 57 – 72.

[20] a) G. Chen, Y. Tan, B. Wu, G. Fu, N. Zheng, *Chem. Commun.* **2012**, *48*, 2758 – 2760; b) B. Wu, N. Zheng, G. Fu, *Chem. Commun.* **2011**, *47*, 1039 – 1041.

[21] M. Xie, Z. Lyu, R. Chen, Y. Xia, *Chem. Eur. J.* **2020**, *26*, 15636 – 15642.

[22] a) C. Wang, H. Daimon, Y. Lee, J. Kim, S. Sun, *J. Am. Chem. Soc.* **2007**, *129*, 6974 – 6975; b) Y. Kang, J. B. Pyo, X. Ye, R. E. Diaz, T. R. Gordon, E. A. Stach, C. B. Murray, *ACS Nano* **2013**, *7*, 645 – 653.

[23] a) H. Zheng, R. K. Smith, Y. Jun, C. Kisielowski, U. Dahmen, A. P. Alivisatos, *Science* **2009**, *324*, 1309 – 1312; b) H.-G. Liao, L. Cui, S. Whitelam, H. Zheng, *Science* **2012**, *336*, 1011 – 1014.

[24] Y. Xiong, J. M. McLellan, Y. Yin, Y. Xia, *Angew. Chem. Int. Ed.* **2007**, *46*, 790 – 794; *Angew. Chem.* **2007**, *119*, 804 – 808.

Manuscript received: September 9, 2020
Revised manuscript received: November 1, 2020
Accepted manuscript online: November 5, 2020
Version of record online: December 23, 2020